AMERICAN SOCIETY FOR MICROBIOLOGY | Applied and Environmental Microbiology

Comparative Analysis of Microbial Communities in Iron-Dominated Flocculent Mats in Deep-Sea Hydrothermal Environments

Hiroko Makita,[a,b] Sakiko Kikuchi,[a] Satoshi Mitsunobu,[c] Yoshihiro Takaki,[a] Toshiro Yamanaka,[d] Tomohiro Toki,[e] Takuroh Noguchi,[f] Kentaro Nakamura,[g] Mariko Abe,[a] Miho Hirai,[a] Masahiro Yamamoto,[a] Katsuyuki Uematsu,[h] Junichi Miyazaki,[a] Takuro Nunoura,[a] Yoshio Takahashi,[i] Ken Takai[a]

Japan Agency for Marine-Earth Science & Technology (JAMSTEC), Yokosuka, Japan[a]; Department of Applied Chemistry, Faculty of Engineering, Kanagawa Institute of Technology, Atsugi, Kanagawa, Japan[b]; Institute for Environmental Sciences, University of Shizuoka, Shizuoka, Japan[c]; Department of Earth Sciences, Okayama University, Okayama, Japan[d]; Department of Chemistry, Biology, and Marine Science, Faculty of Science, University of the Ryukyus, Nishihara, Okinawa, Japan[e]; Center for Advanced Marine Core Research, Kochi University, Nankoku, Japan[f]; Department of System Innovation, Graduate School of Engineering, The University of Tokyo, Tokyo, Japan[g]; Section 1 Geochemical Oceanography, Office of Marine Research Department of Marine Science, Marine Works Japan Ltd., Yokosuka, Japan[h]; Department of Earth Sciences, Graduate School of Science, The University of Tokyo, Tokyo, Japan[i]

ABSTRACT

It has been suggested that iron is one of the most important energy sources for photosynthesis-independent microbial ecosystems in the ocean crust. Iron-metabolizing chemolithoautotrophs play a key role as primary producers, but little is known about their distribution and diversity and their ecological role as submarine iron-metabolizing chemolithotrophs, particularly the iron oxidizers. In this study, we investigated the microbial communities in several iron-dominated flocculent mats found in deep-sea hydrothermal fields in the Mariana Volcanic Arc and Trough and the Okinawa Trough by culture-independent molecular techniques and X-ray mineralogical analyses. The abundance and composition of the 16S rRNA gene phylotypes demonstrated the ubiquity of zetaproteobacterial phylotypes in iron-dominated mat communities affected by hydrothermal fluid input. Electron microscopy with energy-dispersive X-ray microanalysis and X-ray absorption fine structure (XAFS) analysis revealed the chemical and mineralogical signatures of biogenic Fe-(oxy)hydroxide species and the potential contribution of *Zetaproteobacteria* to the *in situ* generation. These results suggest that putative iron-oxidizing chemolithoautotrophs play a significant ecological role in producing iron-dominated flocculent mats and that they are important for iron and carbon cycles in deep-sea low-temperature hydrothermal environments.

IMPORTANCE

We report novel aspects of microbiology from iron-dominated flocculent mats in various deep-sea environments. In this study, we examined the relationship between *Zetaproteobacteria* and iron oxides across several hydrothermally influenced sites in the deep sea. We analyzed iron-dominated mats using culture-independent molecular techniques and X-ray mineralogical analyses. The scanning electron microscopy–energy-dispersive X-ray spectroscopy SEM-EDS analysis and X-ray absorption fine structure (XAFS) analysis revealed chemical and mineralogical signatures of biogenic Fe-(oxy)hydroxide species as well as the potential contribution of the zetaproteobacterial population to the *in situ* production. These key findings provide important information for understanding the mechanisms of both geomicrobiological iron cycling and the formation of iron-dominated mats in deep-sea hydrothermal fields.

Iron is one of the most common elements on Earth and is the fourth most abundant element in the Earth's crust. Iron has a wide range of oxidation states but exists mostly in a +2 or +3 state in the natural environment. The valence of iron depends on the prevailing environmental physicochemical conditions, such as pH, O_2 concentration, and redox potential. Iron occurs in many mineral phases, including (hydr)oxides, carbonates, silicates, and sulfides. The oxidation of ferrous to ferric iron releases energy, which is harnessed by some iron-oxidizing prokaryotes. Ferrous iron is stable under anoxic conditions but can autoxidize in air. Some microbial communities that are unable to use solar energy via photosynthesis use energy from iron oxidation for CO_2 assimilation (1).

Iron-oxidizing chemolithoautotrophs were first identified in the 19th century by Ehrenberg (2) and Winogradsky (3). These microorganisms became important for understanding the global iron cycle (4) and also for industrial applications in biomining (5–7). More recently, interest has increased in iron oxidation and its impacts on biogeochemical elemental cycles in acidic and circumneutral environments under microaerobic and anaerobic conditions (8–15). Recent culture-dependent and -independent microbiological characterizations have revealed that a species of *Zetaproteobacteria*, *Mariprofundus ferrooxydans* (16), and its relatives commonly occur in deep-sea low-temperature hydrothermal

Received 3 May 2016 **Accepted** 11 July 2016

Accepted manuscript posted online 15 July 2016

Citation Makita H, Kikuchi S, Mitsunobu S, Takaki Y, Yamanaka T, Toki T, Noguchi T, Nakamura K, Abe M, Hirai M, Yamamoto M, Uematsu K, Miyazaki J, Nunoura T, Takahashi Y, Takai K. 2016. Comparative analysis of microbial communities in iron-dominated flocculent mats in deep-sea hydrothermal environments. Appl Environ Microbiol 82:5741–5755. doi:10.1128/AEM.01151-16.

Editor: S.-J. Liu, Chinese Academy of Sciences

Address correspondence to Hiroko Makita, makita@jamstec.go.jp.

Supplemental material for this article may be found at http://dx.doi.org/10.1128/AEM.01151-16.

environments around the world. They occur in microbial mats and on altered basalts at the Lō'ihi Seamount (17–23), in microbial mats at the northern Mariana Volcanic Arc, and in the Southern Mariana Trough (24–26), in Fe-(hydr)oxide mats at the Vailulu'u Seamount (27, 28), in the iron-containing flocculent mats in the hydrothermal fields of the Kermadec Arc (29), in the Fe-rich hydrothermal sediments in the South Tonga Arc submarine volcanoes (30), in the Fe-oxide mud at the Red Seamount in the eastern Pacific (31), in the hydrothermal deposits at the Franklin Seamount in the Woodlark Basin (32), in the iron-oxide deposits at the Juan de Fuca Ridge in the Northeast Pacific Ocean (33–36), and in sediments of the near-shore environments of Maine (37).

Mariprofundus ferrooxydans is an iron-oxidizing neutrophilic chemolithoautotroph that produces helical Fe-(oxy)hydroxide "stalks" (16, 38, 39), which morphologically resemble the stalks of *Gallionella* species (2, 40–47). Indeed, helical Fe-(oxy)hydroxide stalks in deep-sea hydrothermal environments were long regarded as potential products of deep-sea *Gallionella* populations (48) until the first isolation of *M. ferrooxydans* (16, 38) (see Table S1 in the supplemental material).

Members of *Zetaproteobacteria* dominate the Fe-(oxyhydr)oxide mat microbial communities in relatively low-temperature hydrothermal fields (25, 26) and also the nearshore marine environment, where they may be associated with mild steel corrosion (37). Although Singer et al. conducted a genomic analysis of *M. ferrooxydans* PV-1 (49), and the biogeographic distribution of deep-sea zetaproteobacterial populations has been investigated in several Pacific submarine hydrothermal systems (50), the distribution, diversity, and function of *Zetaproteobacteria* and iron-oxidizing microbes in the marine environment remain to be determined.

In this study, we investigated four iron-dominated mats and deposits obtained from deep-sea hydrothermal fields in the Northern Mariana Volcanic Arc (the Yellow Top site of the northwestern [NW] Eifuku Seamount) (51), the Southern Mariana Trough (the Snail site and the Urashima site) (52), and the Okinawa Trough (the Fox site of the Tarama Knoll) (53). The abundance and composition of zetaproteobacterial and other potential iron-oxidizing populations in geographically and geochemically distinct iron mat communities were investigated by 16S rRNA gene clone analysis. Moreover, using the X-ray absorption near-edge structure (XANES) technique, the chemical species of iron oxide minerals derived from iron-oxidizing bacteria were determined.

MATERIALS AND METHODS

Sample collection. Mat samples were collected during leg 2 of the NT10-06 cruise (April 2010) of the R/V *Natsushima* (Japan Agency for Marine-Earth Science and Technology [JAMSTEC], Japan) using the remotely operated vehicle (ROV) *Hyper-Dolphin* (JAMSTEC) at the Fox site (25°05.50′N, 124°32.50′E; 1,532 m depth) near the summit of the Tarama Knoll (Fig. 1b) using an M-type sediment sampler (54). Similar mat samples were collected from the Yellow Top site of the Northwest (NW) Eifuku Seamount (21°29.23′N, 144°02.57′E; 1,545 m; Fig. 1c) with ROV *Hyper-Dolphin* and from the R/V *Natsushima* using an M-type sediment sampler during the NT10-13 Leg2 cruise (July to August 2010). Samples from the Snail site (12°57.214′N, 143°37.147′E; 2,849 m depth) and the Urashima site (12°55.30′N, 143°38.89′E; 2,930 m depth) were collected with the deep submersible vehicle (DSV) *Shinkai6500* (JAMSTEC) using an M-type sediment sampler during the YK10-10 cruise (August 2010) of the R/V *Yokosuka* (JAMSTEC). All samples had a soft fluffy texture, were brown or orange-yellow in color, and were likely composed of amorphous Fe-oxides. These samples were stored at −80°C for microbiological and mineralogical analyses. Subsamples were fixed with formalin (final concentration, 3.7%) for microscopic observation and stored at 4°C.

A gas-tight water sampler (WHATS-II) (55) from the ROV or DSV was used to collect fluids for chemical analysis of the mats at all sites. A temperature probe was fixed on the inlet tube to measure and monitor the fluid temperature in real time during sampling. The fluids were collected with a pair of gas-tight bottles, one of which was used for soluble component analysis and the other for gas analysis. Immediately after the water sampler was recovered onboard, the bottle for gas analysis was processed with a vacuum line to retrieve all of the dissolved gasses in the fluids. The fluid samples for soluble component analyses were passed through 0.2- or 0.45-μm-pore-diameter filters to remove particles. The samples for onshore cation analyses were acidified with nitric acid to a pH of <2.

Fluid chemistry and gas composition. The chemical composition of the hydrothermal fluid and ambient seawater (near-bottom water) above the mats was analyzed to understand the local environmental conditions, as described below.

The pH was determined using a pH meter. Gas extraction was performed according to the method of Saegusa et al. (55). The concentrations of H_2, CO_2, and CH_4 were analyzed onshore by gas chromatography with a thermal conductivity detector (TCD) (GL Sciences). The concentration of H_2S was measured by colorimetry using methylene blue (56), and the ammonia concentration was measured by the Nessler method (57). The ferrous iron concentration was determined onboard using a colorimetric method (58). The sulfate concentration was determined by ion chromatography. Other major dissolved elemental species were analyzed in onshore laboratories. Major cation concentrations (Ca and Mg) were measured by inductively coupled plasma-atomic emission spectrometry (ICP-AES).

Scanning electron microscopy and elemental analysis by SEM-EDS. The morphological characteristics of the mat samples were examined by scanning electron microscopy using a field-emission scanning electron microscope (SEM, JSM-6500F; Jeol, Tokyo, Japan) equipped with energy-dispersive X-ray spectroscopy (EDS, JED 2300; Jeol). Dried samples were mounted on a sample stub with double-sided adhesive conductive carbon tape. The samples were coated with osmium using an osmium plasma coater (POC-3; Meiwafosis, Osaka, Japan). EDS was used to estimate the elemental composition of each sample by a semiquantitative method based on the X-ray spectrum produced by the electron beam-sample interaction. The SEM-EDS analysis was conducted at an acceleration voltage of 5 keV for morphological observation and 15 keV for elemental analysis.

XAFS analyses. Bulk Fe K-edge XAFS spectra of the mat samples were measured at the beamline BL01B1 at SPring-8 (Hyogo, Japan) with an Si(111) double-crystal monochromator and two mirrors. Both the extended X-ray absorption fine structure (EXAFS) and the X-ray absorption near-edge structure (XANES) were obtained. All XAFS spectra were obtained in transmission mode. Solid samples were diluted to approximately 1% (wt/wt) using boron nitride (BN) powder. All of the XAFS measurements were conducted at room temperature under ambient air conditions. The XAFS data for Fe were analyzed using the REX2000 software (Rigaku Co., Akishima, Tokyo, Japan). The EXAFS oscillation was extracted from the original spectrum by a spline-smoothing method.

Preparation of reference materials for Fe XAFS analysis. Fe-(oxy)hydroxide reference materials, including two-line ferrihydrite, goethite, hematite, and magnetite, were synthesized by the procedure of Schwertmann and Cornell (1). The mineralogical verification of these Fe-(oxy)-hydroxides was conducted with a powder X-ray diffractometer (XRD, MultiFlex; Rigaku). The other Fe reference materials were purchased from Hori Mineralogy Ltd., Japan.

For comparison with natural deep-sea iron mat samples, biogenic Fe-(oxy)hydroxides were synthesized according to the method of Kikuchi et

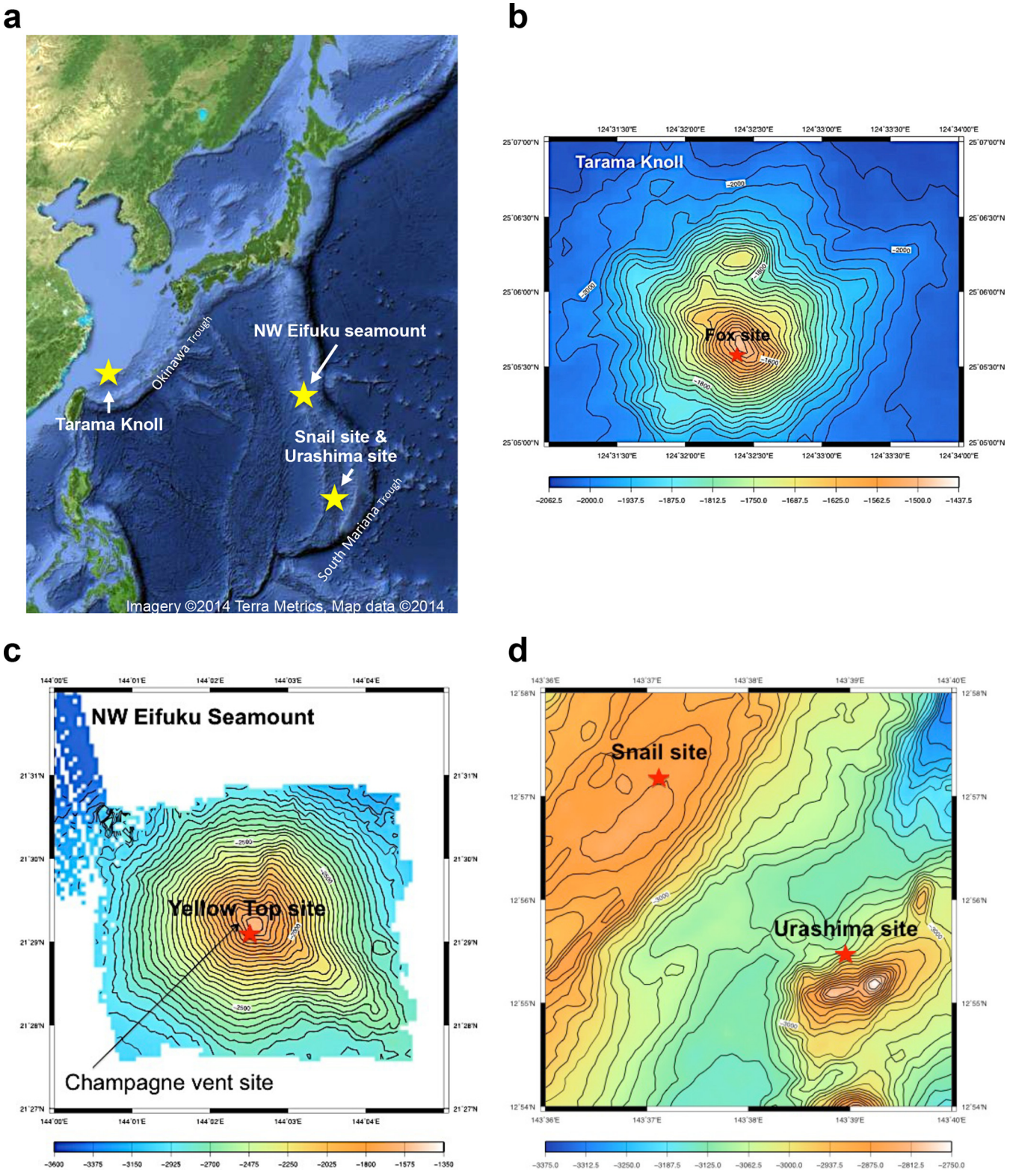

FIG 1 Location of hydrothermal fields studied. (a) A geographic overview of all of the hydrothermal fields, the Urashima and Snail sites in the South Mariana Trough, the NW Eifuku Seamount in the North Mariana Volcanic Arc, and the Tarama Knoll field in the Okinawa Trough. A yellow star indicates the sampling sites. (Base map from Google Maps.) (b to d) Bathymetric maps of the four hydrothermal fields. Red stars indicate the locations where sampling of the iron mats was conducted.

al. (59) using a pure culture of the *Mariprofundus ferrooxydans* type strain PV-1 (ATCC-BAA-1020) (16), obtained from the American Type Culture Collection. *Mariprofundus ferrooxydans* was cultured in artificial seawater containing trace minerals and vitamins (16). FeS was provided as the energy source for bacterial growth. After 24 h of cultivation at 25°C, fluffy Fe-(oxy)hydroxide samples produced by *M. ferrooxydans* were washed with Milli-Q water to remove the medium and used for subsequent analyses.

Cell counting. Prokaryotic cell numbers in the mat samples were determined as previously described (9, 60). To detach the microbial cells from inorganic materials, a sample (approximately 20 mg) was sonicated twice (50 kHz, 100 W) at 25°C for 1 min in an ultrasonic bath (VS-100; Iuchi, Osaka, Japan). Hydrochloric acid was added to the sample at a final concentration of 0.1 M. The sample was then centrifuged at 190 × *g* for 1 min to remove inorganic particles. The supernatant was filtered through a black 0.2-μm-pore-diameter polycarbonate filter (GE Osmonics, USA). To remove acid, the filter was washed twice with phosphate-buffered saline (PBS) (pH 7.4; Life Technologies). Prokaryotic cells on the filter were stained with 4′,6′-diamidino-2-phenylindole dihydrochloride (DAPI) (61), washed twice with PBS, and dried in a sterile covered petri dish. The cells on the filter were counted using a BX51 fluorescence microscope (Olympus, Tokyo, Japan).

DNA extraction, PCR amplification, cloning, and sequencing. DNA was extracted from approximately 5 g of a mat sample from each of the different locations using a PowerMax soil DNA isolation kit (Mo-Bio Laboratories, Solana Beach, CA), according to the manufacturer's instructions. Partial 16S rRNA genes were amplified by PCR using LA *Taq* with LA buffer (TaKaRa Bio, Otsu, Japan). For bacterial 16S rRNA gene amplification, the oligonucleotide primer set of Bac27F (5′-AGAGTTTG ATCCTGGCTCAG-3′) and Uni1492R (5′-ASGGNTACCTTGTTACGA CTT-3′) was used, with 30 cycles of the thermal program (96°C for 25 s, 53°C for 45 s, and 72°C for 120 s) (62). For archaeal 16S rRNA gene amplification, the primer set of Arc21F (5′-TTCCGGTTGATCCYGCC GGA-3′) and Uni1492R was used, with 30 cycles of the thermal program (96°C for 25 s, 50°C for 45 s, and 72°C for 120 s) (62). Gene clone libraries of 16S rRNA were constructed using a TA cloning kit (Invitrogen, Carlsbad, CA, USA). The nucleotide sequences of randomly selected clones were determined with the BigDye Terminator version 3.1 sequencing kit (Applied Biosystems, Foster City, CA, USA) using M13 M4 (5′-GTTTTC CCAGTCACGAC-3′) and M13RV (5′-TGTGGAATTGTGAGCGG-3′) primers on an ABI Prism 3730xl genetic analyzer (Applied Biosystems). The sequences were assembled with Sequencher version 4.8 software (Gene Code Corporation, Ann Arbor, MI, USA). The most similar reference sequences were retrieved from the RDP and the GenBank database (63, 64).

Phylogenetic analyses. After chimeric sequences were removed using the RDP chimera check program (65), distance matrices were generated from the alignment data sets from each clone library using ARB (66) or MEGA 5 (67) with the neighbor-joining method (68) and maximum-likelihood method (69). Clones of >97% sequence similarity were grouped into the same phylotype using Sequencher 4.8 based on the distance matrix. Then, representative phylotypes were realigned with sequences in public databases, including the closest sequence determined by BLAST (70). All sites with gaps in the alignment data sets were removed using MEGA 5. A maximum-likelihood tree was constructed using MEGA 5. Bootstrap values were estimated using 1,000 replicates.

Quantitative PCR. Prokaryotic, archaeal, and zetaproteobacterial 16S rRNA gene copy numbers were estimated in whole DNA assemblages from mat samples using the quantitative PCR (qPCR) assay developed by Takai and Horikoshi (71) and Kato et al. (26), using the 7500 real-time PCR system (Applied Biosystems, Foster City, CA, USA).

The primers were Uni340F (5′-CCTACGGGRBGCASCAG-3′) and Uni806R (5′-GGACTACNNGGGTATCTAAT-3′) for the prokaryotic universal 16S rRNA gene, Arch349F (5′-GYGCASCAGKCGMGAAW-3′) and Arch806R (5′-GGACTACVSGGGTATCTAAT-3′) for the archaeal 16S rRNA gene, and Zeta672F (5′-CGGAATTCCGTGTGTAGCAGT-3′) and Zeta837R (5′-GCCACWGYAGGGGTCGATACC-3′) for the zetaproteobacterial 16S rRNA gene.

The TaqMan probes were Uni516F (5′-TGYCAGCMGCCGCGGTA AHACVNRS-3′) for the prokaryotic universal 16S rRNA gene, Arch516F (5′-TGYCAGCCGCCGCGGTAAHACCVGC-3′) for the archaeal 16S rRNA gene, and Zeta705T (5′-TATACGGAGGAACACCWGAGGC-3′) for the zetaproteobacterial 16S rRNA gene.

The following thermal programs were used: for the quantification of prokaryotic 16S rRNA gene numbers, initial steps were 96°C for 1 min and then 50 cycles of 96°C for 25 s and 57°C for 6 min; for archaeal 16S rRNA gene number, initial steps were 96°C for 1 min and then 50 cycles of 96°C for 25 s and 59°C for 6 min; and for the zetaproteobacterial 16S rRNA gene number, initial steps were 50°C for 2 min and then 95°C for 10 min, followed by 40 cycles of 95°C for 15 s and 60°C for 1 min. Standard curves for the quantification of prokaryotic and archaeal 16S rRNA genes were prepared according to a previously published method (71). A dilution series of plasmid DNA with a zetaproteobacterial 16S rRNA gene insertion obtained from the mat samples in this study was used as a qPCR standard for zetaproteobacterial 16S rRNA gene quantification. The abundance of each targeted gene in the DNA assemblage was determined as an average of the results from triplicate analyses.

Accession number(s). The 16S rRNA gene sequences representing the operational taxonomic units (OTUs) used in this analysis were submitted to GenBank and assigned the accession numbers LC086656 through LC086682.

RESULTS AND DISCUSSION

Site description and sample collection. (i) Fox site (Tarama Knoll). The Fox site at the Tarama Knoll is located near the summit at a water depth of 1,530 to 1,540 m (Fig. 1a and b). At this site, the seafloor is covered with an orange-brown mat >30-cm thick across an area greater than 100 m^2 (53). The sediments were predominantly orange-brown and rusty-brown and consisted of ferrihydrite or possibly microcrystalline goethite. The sediment surface was orange, which suggests the occurrence of dense filamentous microbial mats (Fig. 2a and b). In addition, some thin chimneys (approximately 30 cm in height) were occasionally observed. The temperature of the sediment was approximately 6°C higher than that of the ambient bottom water, which was 3.8°C. The temperature of the diffusing hydrothermal fluids at the Fox site was as high as 20°C (Table 1). Mineralogical and microbiological analyses were conducted at the surface zone of the iron mats (sample identification [ID] TMm).

(ii) Yellow Top site (NW Eifuku Seamount). The NW Eifuku Seamount is located on the northern Mariana Volcanic Arc. It is a roughly conical basaltic volcano, with a basal diameter of approximately 9 km (Fig. 1a and c). The CO_2-rich hydrothermal vent site named the Champagne vent site is on the southwestern side of the seamount at a depth between 1,570 m and 1,607 m (Fig. 1c) (50, 72, 73). Orange mats were located around this vent site and were widespread from the summit to the narrow ridges extending from the summit (Fig. 1c). The sediment sample from the summit area (Yellow Top site) was fragile and had a fluffy texture. According to Nakamura et al. (74), it was likely composed of amorphous silica and Fe oxides (74). Black basaltic gravels were present below the sediment. At the surface, the bright-orangeish mat consisted of dense microbial filaments (Fig. 2c). The surface zone of the mat (sample ID NMS) was subjected to further analyses.

(iii) Snail site (Southern Mariana Trough). The Snail site is situated in the southwestern Mariana Trough (Fig. 1a and d) (75–78). Extensive Fe-oxide-encrusted rock and abundant mat mate-

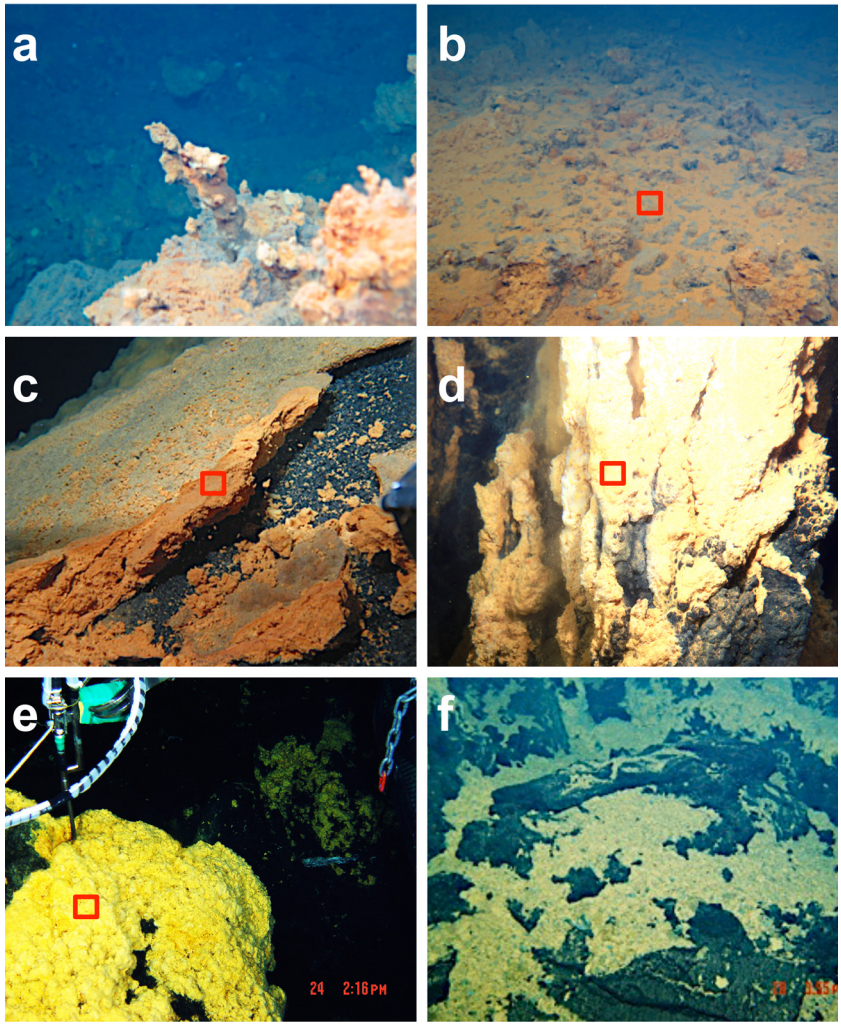

FIG 2 Photographs of the iron-dominated mats and deposits collected by the ROV *Hyper-Dolphin* and the DSV *Shinkai6500*. (a) Iron chimney of the Tarama Knoll Fox site. (b) Iron mat of the Tarama Knoll Fox site. (c) Iron-dominated mats of the NW Eifuku Seamount Yellow Top site. (d) Fe-(hydr)oxide chimney of the Urashima site. (e) Iron mats of the hydrothermally active areas at the Snail site. (f) Iron mats of the hydrothermally inactive areas of the Snail site. The red squares indicate the analyzed areas in panels b to e.

rials are in the western part of the Snail site (Fig. 2e and f). The mat materials were bright yellow, different from the colors of the mats at the other sites. The surface of the mat was whitish-yellow, suggesting an abundance of microbial filaments containing goethite. There was no chimney structure and no evident hydrothermal fluid discharge found in this area, whereas a temperature anomaly up to 50°C was recorded within the sediments in several hydrothermally active areas (Table 1). Although the temperature was not measured in all of the iron mats, most of the iron mat deposits appeared to occur in the hydrothermally active area (Table 1). A representative iron mat from the hydrothermally active site (sample ID SAM) was subjected to further analyses.

TABLE 1 Sample characteristics of iron mats from various hydrothermal fields

Site	Sample type	Sample for fluid analysis	Temp (°C)	pH	Soluble Fe concn (μM)	Cell density (g [wet wt])	Copy no. of 16S rRNA gene in:		
							Prokaryotes	*Archaea* (Arc/Prok [%])[a]	*Zetaproteobacteria* (Zeta/Prok [%])[b]
Tarama Knoll	Sediment	Hydrothermal fluid	20	6.4	0.08–140	1.12×10^8	1.75×10^9	5.65×10^8 (32)	7.17×10^7 (4)
NW Eifuku Seamount	Sediment	Near-bottom water	2.7	7.4	70–140	2.23×10^8	1.83×10^9	4.55×10^8 (25)	1.04×10^8 (6)
Snail site	Sediment	Hydrothermal fluid	27–64.5	6.9	4.8–80	1.06×10^8	8.56×10^8	4.98×10^8 (58)	1.46×10^7 (2)
Urashima site	Chimney-like	Hydrothermal fluid	56–76	5.7	106–151	1.90×10^8	2.03×10^9	1.76×10^8 (9)	2.64×10^8 (13)

[a] Arc/Prok, ratio of prokaryotic and archaeal 16S rRNA gene copy numbers.
[b] Zeta/Prok, ratio of prokaryotic and zetaproteobacterial 16S rRNA gene copy numbers.

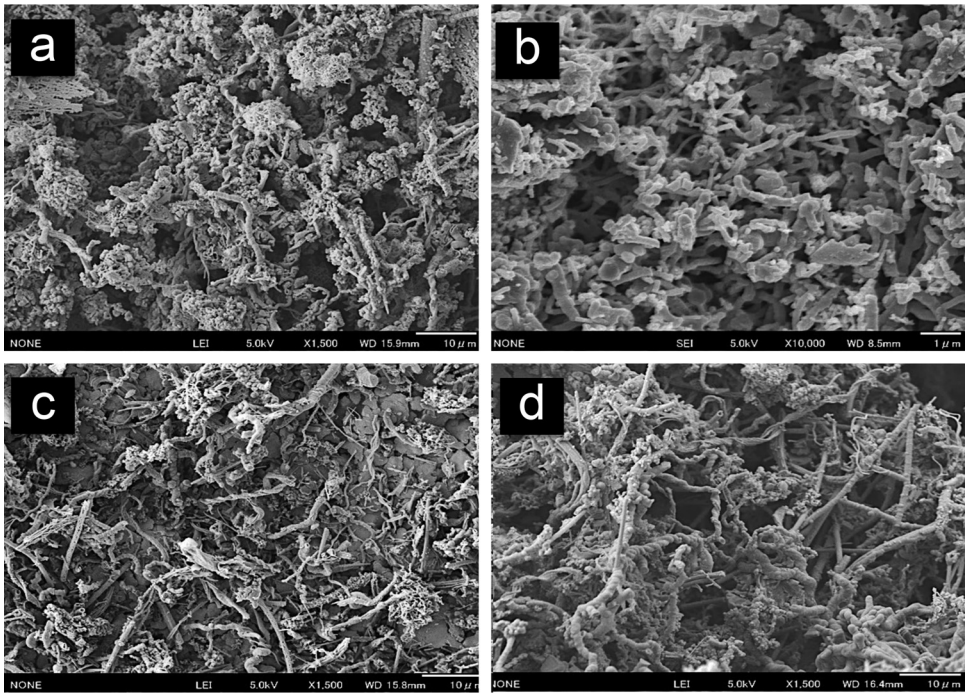

FIG 3 SEM images of iron-dominated mat samples. (a) Iron mats from the Tarama Knoll Fox site. (b) Iron mats from the NW Eifuku Seamount Yellow Top site. (c) Iron chimney sample from the Urashima site. (d) Iron mats from the hydrothermally active areas of the Snail site. Scale bars, 10 μm (panels a, c, and d) or 1 μm (panel b).

(iv) Urashima site (Southern Mariana Trough). The Urashima hydrothermal field is located in the Southern Mariana Trough, at a depth of 2,930 m (Fig. 1a and d). This field was found in the year 2010 during the YK10-10 cruise by the DSV *Shinkai6500* (52, 79, 80). Orange chimneys approximately 10-m high were observed throughout the site (Fig. 2d). These chimney structures were very friable. They were predominantly bright orange, suggestive of ferrihydrite or possibly of microcrystalline goethite, with lighter-orange tops possibly composed of dense fibrous microbial mats. The sampled chimney had diffusing fluid at the top. A temperature anomaly (76°C maximum) was measured inside the chimney by inserting a probe into the chimney (Table 1). The surface of the chimney (sample ID UCSW) was studied in detail. The interior of the chimney was sampled to determine the elemental and mineral composition.

SEM and chemical analysis by SEM-EDS. The mat samples from all of the sites were examined by scanning electron microscopy (SEM). Distinctive structures, such as helical twists, plaits, and filaments, were observed in almost all samples (Fig. 3a to d). The observed helically twisted and plate-like materials, which are called stalks, resembled the typical biogenic Fe-rich (oxyhydr)oxides produced by neutrophilic Fe-oxidizing bacteria, such as *Mariprofundus ferrooxidans* (16, 39, 81) and *Gallionella ferruginea* (41, 44, 82, 83). Furthermore, SEM-EDS analysis showed that the distinctive stalk-like structures in the iron mat materials from all sites were mainly composed of Si, Fe, and O (see Table S2 in the supplemental material), indicating that the stalk-like structures contained iron oxide. The SEM observations indicated that the iron oxide extensively covered the stalk-like structures. Microbial cells associated with the stalk structures were rarely observed. The SEM-EDS analysis revealed that Fe was widely distributed around the stalk-like structures (see Fig. S1 in the supplemental material), but the density of Fe was highly varied on the microscale of the iron mat materials (Fig. 3).

XAFS analyses. The chemical speciation and characteristics of Fe in the mat samples were determined using Fe EXAFS analysis (Fig. 4). The Fe EXAFS features of mat samples from the Tarama Knoll Fox site, the NW Eifuku Seamount Yellow Top site, and the Urashima and the Snail sites were similar to those of the Fe(III)-(oxy)hydroxides, with short range-ordered Fe-O_6 and two-line ferrihydrite, and were significantly different from those of other Fe species, including Fe(II) (magnetite, siderite, fayalite, and pyrite) and crystalline Fe(III)-(oxyhydr)oxides (hematite, goethite, and lepidocrocite). This result indicated that the mat samples were mainly composed of short-ordered Fe(III)-(oxy)hydroxides, which was consistent with the SEM-EDS findings. In the Fe EXAFS features, remarkable differences were found between the two-line ferrihydrite and the mat Fe(III)-(oxy)hydroxides. Although two small peaks at k of 5.0 to 5.2 $Å^{-1}$ and 7.0 to 7.5 $Å^{-1}$ were observed in the two-line ferrihydrite (Fig. 4a, enlarged view), these peaks were not found in all of the mat samples. Previous studies have shown that peaks at k of 5.0 to 5.2 $Å^{-1}$ and 7.0 to 7.5 $Å^{-1}$ were predominantly derived from Fe-Fe coordination in the Fe(III)-(oxy)hydroxides and two-line ferrihydrite (84, 85). Using EXAFS analyses, Edwards et al. (23) also showed that the biogenic Fe(III)-(oxy)hydroxides are composed of short-ordered Fe-O_6 linkages, which are normally not observed in abiotically synthesized Fe(III)-(oxy)hydroxides (e.g., two-line ferrihydrite). Previous studies by Edwards et al. (23) were conducted using a deep-sea sample, as was done in this study.

Fourier-transform (FT) analyses of the EXAFS spectra of the two-line ferrihydrite and mat samples are shown in Fig. 4b (phase-

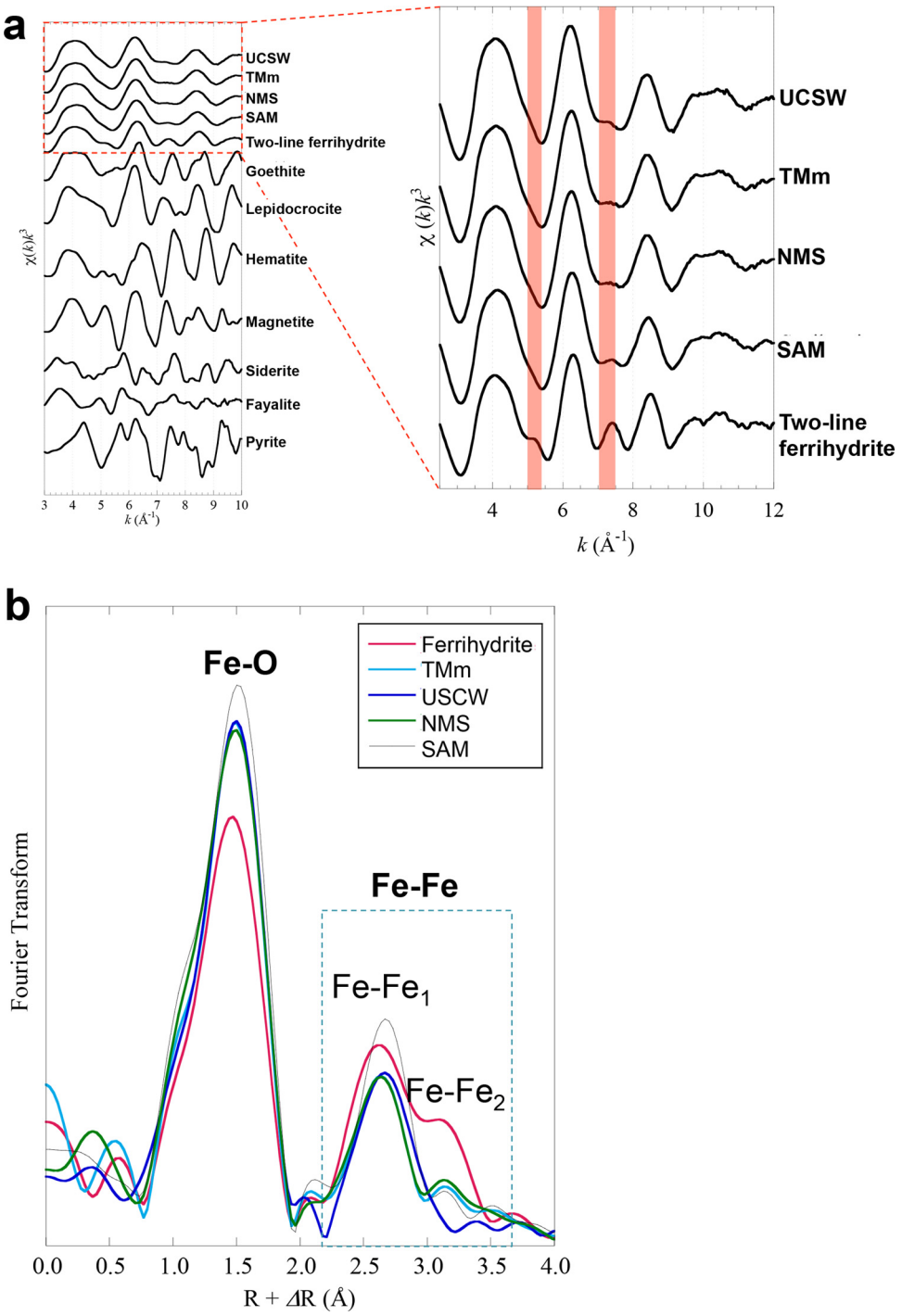

FIG 4 EXAFS spectra and Fourier-transformed data of the iron mat samples. (a) Normalized k^3-weighted EXAFS spectra for iron mat samples and reference minerals at the iron K-edge. (b) Radical structure function of the spectra shown in panel a after a Fourier transformation of k ranging from 3 $Å^{-1}$ to 10 $Å^{-1}$.

shift uncorrected). The first shell at 1.5 Å and the second shell at 2.2 to 3.5 Å correspond to the Fe-O and Fe-Fe coordination, respectively (84). In the FT of two-line ferrihydrite, the Fe-Fe shells contained two peaks corresponding to edge sharing of the Fe-O_6 octahedron (Fe-Fe_1) at 2.2 to 2.8 Å and corner-sharing (Fe-Fe_2) at 2.8 to 3.5 Å in the Fe-Fe linkages (Fig. 4b) (84). In contrast, the mat Fe(III)-(oxy)hydroxides were predominantly composed of Fe-Fe edge-sharing linkages. Mitsunobu et al. (85) and Toner et al. (86) also found a predominance of edge-sharing linkages in the crystal structure of biogenic Fe(III)-(oxy)hydroxides. They suggested that this feature may be used as a structural signature for biogenic Fe(III)-(oxy)hydroxides. The results of the EXAFS analysis indicated that most of the Fe(III)-(oxy)hydroxides in the iron mats in geographically and geologically distinct hydrothermal systems

TABLE 2 Taxonomic affiliation of bacterial 16S rRNA gene clones from iron mat samples in different deep-sea hydrothermal systems

Taxonomic affiliation	Iron mats at Fox site of Tarama Knoll (TMm)	Surface deposits in Yellow Top site of NW Eifuku Seamount (NMS)	Hydrothermally active mats at Snail site (SAM)	Chimney surface at Urashima site (UCSW)
Acidobacteria	2	1		1
Actinobacteria				
Bacteroidetes		5		2
BD1-5		4	1	3
Chlorobi		1		1
Chloroflexi	1	1	7	
Cyanobacteria	1			
Deferribacteres	3		2	
Deinococcus-Thermus				1
Elusimicrobia		1		
EM19			13	
Fibrobacteres		1		
Firmicutes				
Fusobacteria	2	2		
Gemmatimonadetes				
JL-ETNP-Z39			1	
Nitrospinaceae	6	2	2	1
Nitrospirae	4		13	2
Planctomycetes	9		7	
TA06	2			
Thermotogae			5	
TM6	1			
Verrucomicrobia	1			
Alphaproteobacteria	6	8	5	7
Betaproteobacteria		1		
Gammaproteobacteria	14	22	11	23
Deltaproteobacteria	27	10	10	16
Epsilonproteobacteria				7
Zetaproteobacteria	8	21	8	75
Unknown *Proteobacteria*		8	3	2
Candidate division BRC1		3	1	
Candidate division OD1		1		1
Candidate division OP10	1			1
Candidate division OP11				1
Candidate division OP3			1	
Candidate division WS3	1			1
Candidate division WS6				1
Total clones	89	92	90	146

were produced by microbial processes, likely by similar or common functions of iron-oxidizing components in the iron mat microbial community.

Abundance and phylotype composition of the microbial community in iron-dominated mats. The prokaryotic cell density in the iron-dominated mat material was estimated by direct cell counting using fluorescence microscopy and quantitative PCR (qPCR) of 16S rRNA genes in the environmental DNA assemblages (Table 1). The cell density in the iron mat samples (1.1×10^8 to 2.2×10^8 cells g^{-1} of sediment) was much greater than in the ambient seawater samples (e.g., 1.51×10^4 to 4.30×10^4 cells ml^{-1} at Southern Mariana Trough [Fuchida et al. {87} and our unpublished data]; 6.22×10^3 to 4.8×10^4 cells ml^{-1} at the Indian ocean [Noguchi et al. {88}]). The prokaryotic 16S rRNA gene copy number was greater than the cell density in all iron mat samples, but the abundance patterns in the samples were similar between the prokaryotic 16S rRNA gene copy number and the cell density (Table 1). The qPCR analysis for the zetaproteobacterial 16S rRNA gene also showed a similar pattern in the whole prokaryotic 16S rRNA gene clone analysis (Table 1). The qPCR analysis showed much lower abundance of archaeal 16S rRNA genes than bacterial genes, and the archaeal 16S rRNA gene clone analysis indicated that the predominant archaeal population belonged to *Thaumarchaeota*, which was potentially involved in nitrification in the microbial community (Tables 1 and 2 and Fig. 5) (89). So far, no iron-oxidizing archaea are known from such a deep-sea environment. The results of the archaeal populations and phylotypes are therefore not discussed further in this study.

Four clone libraries of bacterial 16S rRNA genes were constructed from the iron-dominated mat samples from the four hydrothermal fields. Overall, the representative phylotypes found in the bacterial 16S rRNA gene clone libraries from the iron-dominated mats were phylogenetically affiliated with 7 major groups: *Alpha-*, *Gamma-*, *Delta-*, *Epsilon-*, and *Zetaproteobacteria*; *Nitrospira*; and *Planctomycetes* (Table 2). In all of the iron mats, alpha-, gamma-, delta-, and zetaproteobacterial phylotypes were com-

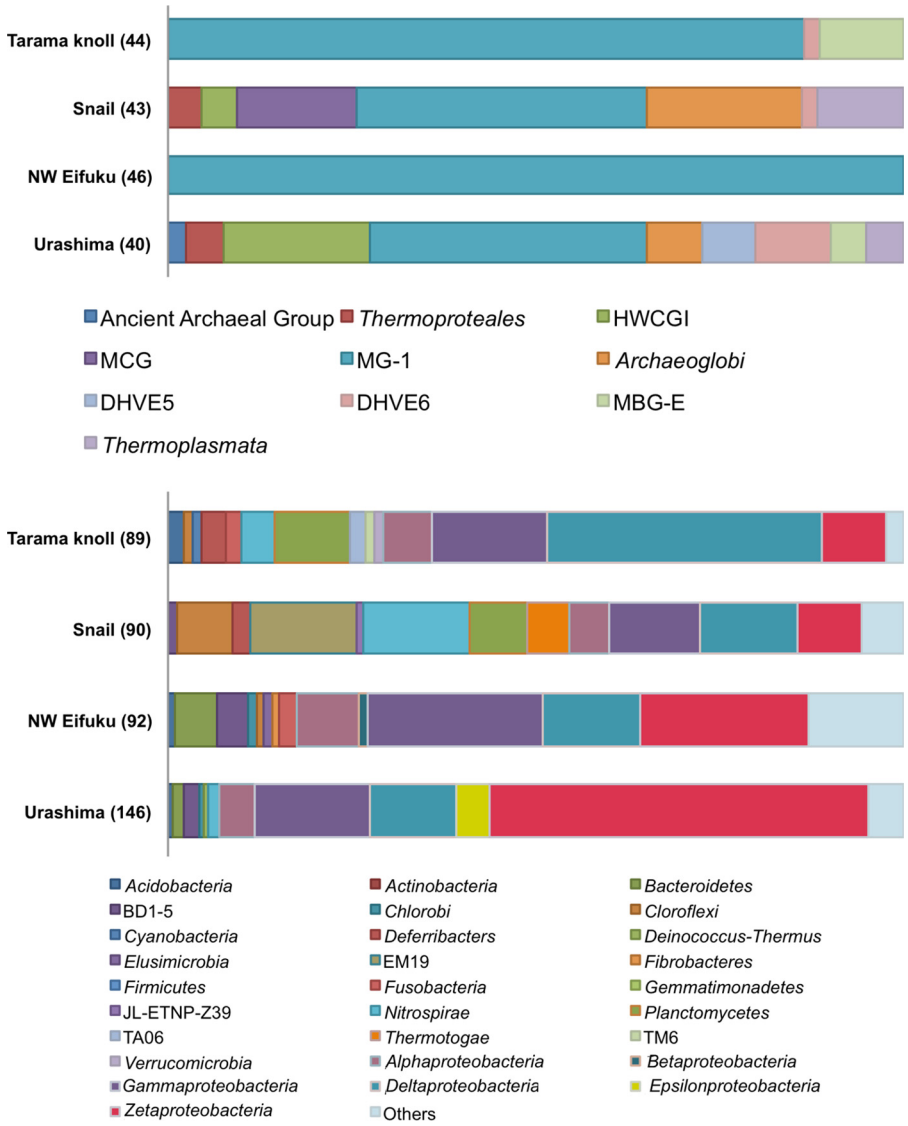

FIG 5 Archaeal and bacterial 16S rRNA gene community structures obtained by the clone analysis of iron mats from Tarama Knoll, the NW Eifuku Seamount, the Snail site, and the Urashima site. The numbers of sequenced clones in each clone library are shown in parentheses. MCG, uncultured miscellaneous crenarchaeotal group; DHVE5 and DHVE6, deep-sea hydrothermal vent euryarchaeotic groups 5 and 6; MGI, marine group I thaumarchaeota; HWCGI, hot-water crenarchaeotal group I; MBG-E, marine benthic group E euryarchaeota; BD1-5, EM19, JL-ETNP-Z39, TA06, and TM6, uncultured bacterial candidate divisions.

monly detected. The relative species richness in each sample was determined through rarefaction analysis (90). The rarefaction curves were constructed by DOTUR (91). The rarefaction curve was not saturated for all samples (see Fig. S2 in the supplemental material), indicating that the entire ecosystems present in each iron mat have not been completely characterized. Consequently, more detailed analyses, including next-generation sequencing, are required to assess the phylogenetic diversity of bacterial components in the iron mat community ecosystems in the future.

The phylotype composition of each iron mat revealed the presence of a phylogenetically diverse bacterial community in iron-dominated mats affected by proximal hydrothermal fluids. Phylotype richness of a microbial community has also been reported from culture-independent molecular analyses of various submarine iron-dominated microbial mats (17, 18, 24–26, 28, 29, 30, 37). The zetaproteobacterial phylotypes represented approximately 1 to 50% of the clonal abundance in the mat samples (Table 2).

In the chimney surface iron mat of the Urashima site, the zetaproteobacterial phylotypes represented the most predominant population in the clone library (Table 2). The relatively high abundance of zetaproteobacterial phylotypes was also indicated by qPCR estimation (Table 1). The *Methylothermus* phylotypes of the *Gammaproteobacteria* were the second most predominant population (Table 2; see also Table S3 in the supplemental material). *Methylothermus* is a thermophilic genus (92). Thus, the presence of the *Methylothermus* phylotypes may be a microbiological signature indicating the occurrence of a relatively high-temperature habitat affected by hydrothermal fluid flow.

The bacterial 16S rRNA gene library from the surface iron mat

sample from the NW Eifuku Seamount was dominated by putative iron-oxidizing zetaproteobacterial phylotypes. Because the physical and chemical properties of the near-bottom water in the Yellow Top site iron-rich sediments of the NW Eifuku Seamount indicated a relatively low input of hydrothermal fluid (Table 1), the predominant bacterial phylotypes may not have been directly associated with the reduced iron and sulfur sources from the hydrothermal fluid. However, the CO_2-enriched acidified fluid derived from the Champagne vent site of the NW Eifuku Seamount may play an important role in providing reduced iron and sulfur sources by leaching the reduced iron and sulfur minerals from the basaltic gravel-like basalt underlying the iron mat sediments.

The bacterial 16S rRNA gene clone library from the Tarama Knoll iron mats was dominated by deltaproteobacterial phylotypes. The most predominant phylotypes within *Deltaproteobacteria* were from the uncultivated environmental group DTB-120 (see Table S4 in the supplemental material). The zetaproteobacterial phylotypes represented 9% of the clonal abundance in the bacterial 16S rRNA gene clone library (Table 2) and 4% of the entire prokaryotic 16S rRNA gene copy number (Table 1). The temperature of the hydrothermal fluid potentially contributed to the iron mat formation and was found to be 20°C. The Fe concentration in the fluid was relatively high (Table 1). These physical and chemical characteristics are likely suitable for biomass production by iron-oxidizing chemolithotrophs, such as the zetaproteobacterial population. Conversely, the bacterial phylotypes closely related to the previously known Fe(III)-, sulfur-, and sulfate-reducing bacteria were not found in the library from the Tarama Fox site, which could recycle ferrous iron from the Fe(oxy)hydroxide minerals (Table 2; see also Tables S3 to S5 in the supplemental material). However, microbial groups of an unknown function (DTB-12, etc.) may have been involved in the recycling of iron in the Tarama Knoll iron mat.

At the Snail site, we investigated the iron mats collected from hydrothermally active areas that had a relatively high temperature and Fe concentration anomalies in the hydrothermal fluid. The 16S rRNA gene sequences related to *Nitrospira*, *Gammaproteobacteria*, *Deltaproteobacteria*, and the uncultivated environmental group EM19 were detected as the predominant phylotypes in the hydrothermally active mat library (see Tables S3 to S5 in the supplemental material). Quantitative PCR analysis indicated that the zetaproteobacterial 16S rRNA gene copy number represented approximately 2% of the entire prokaryotic 16S rRNA gene copy number in the mat sample (Table 1).

These results suggest that the abundance and function of the zetaproteobacterial population are varied in the widespread iron-dominated mats in deep-sea hydrothermal fields and are sensitive to local variations in the physical and chemical conditions in the iron mat structure.

In this study, we found that *Zetaproteobacteria* in the iron-dominated mats and deposits of geographically, geologically, and geochemically different hydrothermal systems were ubiquitous and abundant and also phylogenetically diverse. The zetaproteobacterial phylotypes in the iron mats of the chimney at the Urashima site represented the most dominant population in the bacterial 16S rRNA gene clone library. Almost all of the phylotypes were affiliated with a group represented by the phylotype UCSW-34 (43 clones) of *Zetaproteobacteria* (Fig. 6). Thus, this group of *Zetaproteobacteria* may have a certain niche preference for hydrothermal habitats, such as the Fe-(oxy)hydroxide-containing mat of the chimney at the Urashima site.

On the other hand, the SAM-34 phylotype was the most dominant zetaproteobacterial phylotype in the hydrothermally active iron mat library of the Snail site and was closely related to the environmental clones of Papm3BL23, Papm3BL17, and Papm3BL58 that were previously reported from similar iron mats at the Snail site (26). This lineage of zetaproteobacterial phylotypes was specifically recovered from the iron-dominated microbial communities of the Snail site. The iron mat deposits of NW Eifuku Seamount and Tarama Knoll were both characterized by a relatively low temperature and a possible CO_2-enriched fluid input (Table 1; see also Table S6 in the supplemental material). Thus, the phylogenetic relatedness of the zetaproteobacterial phylotypes may be a reflection of their ecophysiological response to the physical and chemical conditions in their habitats.

Although the phylogenetic diversity of *Zetaproteobacteria* has not yet been fully explored in geographically widespread deep-sea hydrothermal environments, the phylogenetic affiliation of region-specific phylotypes may represent a possible biogeographic divergence of *Zetaproteobacteria*. Based on a culture-independent molecular analysis, McAllister et al. (50) suggested that the phylogenetic diversity of *Zetaproteobacteria* in the Pacific deep-sea hydrothermal system is associated with biogeographic connectivity.

Since the first isolation of the zetaproteobacterium *M. ferrooxydans* from the Lō'ihi Seamount (16), the successful isolation of *M. ferrooxydans* strains has recently been reported (e.g., isolated from a salt marsh on Great Salt Bay, Newcastle [37], and Spillway site, Lō'ihi Seamount [50]). However, the physiological diversity of *Zetaproteobacteria* other than *M. ferrooxydans* remains unknown. To understand the biogeographic distribution and ecophysiological function in global deep-sea environments, the isolation and physiological characterization, as well as the determination of the phylogenetic diversity of *Zetaproteobacteria*, are necessary.

Formation of biogenic Fe-(oxy)hydroxides at the seafloor. Fe-(oxy)hydroxide minerals are among the most abundant products of the weathering of the ocean crust and the alteration of crustal hydrothermal fluid. Although a significant contribution of the subseafloor and seafloor microbial communities to ocean crust alteration and weathering has been indicated (4, 93), it is very difficult in most cases to estimate the microbial contribution to Fe-(oxy)hydroxides formed on the seafloor at the expense of the ocean crust. The readily recovered iron-dominated mats and deposits from the low-temperature hydrothermal environment on the seafloor provide an excellent opportunity to study the indigenous microbial communities and their contribution.

The distinctive morphological and chemical features of the iron-containing minerals demonstrated by SEM-EDS and XAFS analyses, i.e., a filamentous structure encrusted by poorly ordered Fe-(oxy)hydroxides produced by *Gallionella*, *Mariprofundus*, and *Leptothrix* species (39, 43, 46, 81–83, 94), suggest a predominant occurrence and function of iron-oxidizing chemolithotrophs in all of the iron-dominated mats and deposits investigated in this study. The significance of *Zetaproteobacteria*, including *Mariprofundus* spp., in the marine iron mat microbial community has often been inferred from the morphological signature of potentially biogenic Fe-(oxy)hydroxide minerals (39, 93, 94) and has been compared with that of other iron-oxidizing genera in the

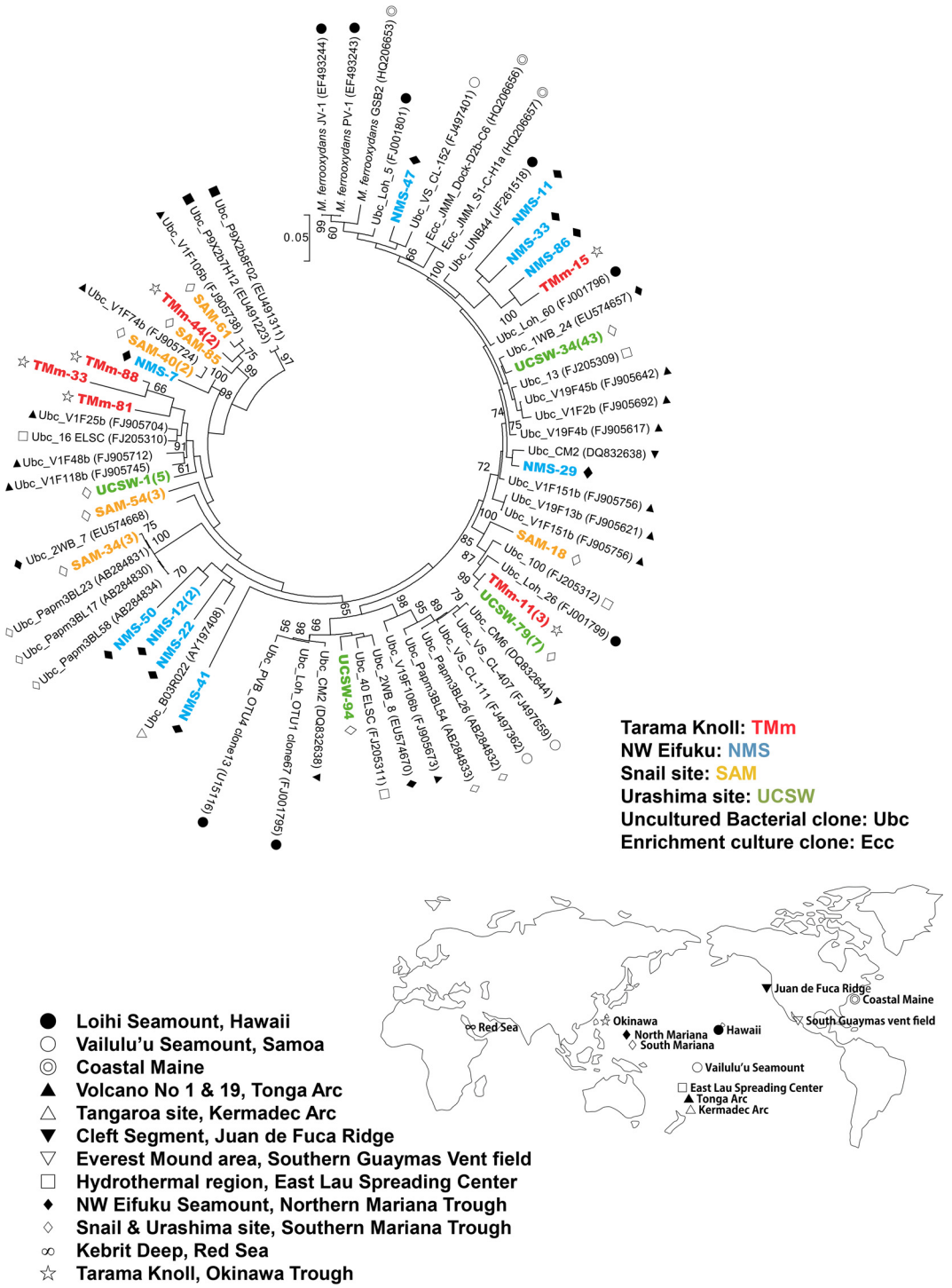

FIG 6 Maximum-likelihood phylogenetic tree of zetaproteobacterial 16S rRNA genes. The 16S rRNA gene clone sequences obtained in this study and the sequence data obtained from the ARB-SILVA database are included in this phylogenetic tree. Unambiguously aligned 1,312-bp nucleotide positions were used for the construction of the phylogenetic tree. Each symbol on the right or left side of a sequence name indicates the geographic location where each clone was obtained. The scale bar represents 5 nucleotide substitutions per 100 positions. Only bootstrap values of >50% are shown. Clones detected in this study are shown in color.

terrestrial environment, such as *Gallionella* and *Leptothrix* (44, 45, 95). In the iron-dominated mat samples in this study, *Zetaproteobacteria* were ubiquitously found in the 16S rRNA gene clone analysis. These results suggest that the potentially biogenic Fe-(oxy)hydroxide minerals in the iron-dominated mats and deposits are produced by the *in situ* function of the zetaproteobacterial component.

Zetaproteobacteria likely use ferrous iron as an electron donor

TABLE 3 Similarities of the EXAFS spectrum between synBIOS, abiotic ferrihydrite, and Fe-(oxyhydr)oxide samples of each iron mat site

Fe-(oxyhydr)oxide sample site	synBIOS (%)[a]	Abiotic ferrihydrite (%)
TMm	88	12
NMS	64	36
SAM	98	2
UCSW	90	10

[a] synBIOS, synthetic biogenic iron oxides derived from *M. ferrooxydans* PV-1, which was cultured at laboratory.

in their energy metabolism and produce complex Fe-(oxy)hydroxide structures as a sink for the resultant ferric iron, which is deposited on an exopolysaccharide stalk. According to SEM-EDS analysis, the elemental compositions of the stalks were very similar in all of the iron mat samples. Interestingly, the predominant mineral composition and stalk structure were very similar to those of the entire chimney structure (from the inside to the surface zone) of the Urashima site (see Fig. S1 in the supplemental material). The Fe-(oxy)hydroxide-encrusted stalk structure was thicker in the inner zone of the chimney (see Fig. S1). The morphological and chemical characteristics of the Fe-(oxy)hydroxide minerals suggest that the Fe-(oxy)hydroxide minerals in the chimney of the Urashima site are mostly biogenic, formed as a function of the predominant *Zetaproteobacteria* population.

It is difficult to judge whether the distinctive iron oxide was formed chemically or biologically based on morphology alone. It has been noted that the helical structure can be chemically formed (96, 97). However, a very specific chemical reaction is necessary to create the helical form, as indicated by García-Ruiz et al. (97). Moreover, the major component of the chemically produced helical structure is a barium-containing silica-carbonate. Thus, both morphological and compositional characteristics would be useful for discriminating between the biogenic iron oxide materials and the abiotically produced materials.

Based on an EXAFS analysis, Kikuchi et al. (59) recently compared a natural iron mat sample collected from the Yellow Top site of the NW Eifuku Seamount with the synthetic biogenic Fe-(oxy)hydroxides (synBIOS) from a culture of *M. ferrooxydans*. They also showed that the primary mineral constituent of both of the Fe-(oxy)hydroxides was ferrihydrite. The two Fe-(oxy)hydroxides exhibited very similar oscillation in *k* space. Using the same method, we found that the deep-sea iron mat samples resembled the synBIOS from *M. ferrooxydans* more than the abiotic ferrihydrite (Table 3). Chan et al. (39) and Kikuchi et al. (81) demonstrated that the synBIOS of *M. ferrooxydans* was several nanometers in size and contained organic carbon. Toner et al. (86) also showed that iron mats obtained from the Lō'ihi Seamount hydrothermal field were composed of nanoparticulate ferrihydrite (Fh)-like phases with short-range structural order (Fh_{SRO}). Moreover, pair distribution function analyses showed that the Fh_{SRO} particles were coated with poorly ordered Si. The Fh_{SRO} in the iron mats of Lō'ihi Seamount was not transformed to other Fe mineral phases during freezing, drying, and aging in seawater for up to 1 year, not even by heat treatment under oxidative conditions (98). Picard et al. (99) demonstrated that the twisted stalk morphology was preserved at high temperature and pressure (250°C, 140 MPa). These results revealed that biogenic Fe-(oxy)hydroxides in the natural iron-dominated mats and deposits may be stable under oxidative conditions, even long after formation. The cooccurrence of biogenic Fe-(oxy)hydroxides and uncultivated zetaproteobacterial populations in deep-sea iron mats may be evidence that the biogenic Fe-(oxy)hydroxides were generated by *Zetaproteobacteria*.

The variability in the abundance and diversity of zetaproteobacterial members of the iron mat microbial community, as observed in the 16S rRNA gene clone analysis in this study, may be related to the physical and chemical conditions of their environment (e.g., the extent of the hydrothermal fluid input) and also with the temporal conditions of iron mat formation (e.g., the aging and generation-preservation stages of the iron mats). Thus, polyphasic environmental, mineralogical, and microbiological study approaches, such as fluid chemistry, XAFS, and culture-independent molecular analyses, are important for a comprehensive understanding of the microbial impact on the formation of Fe-(oxy)hydroxides in deep-sea hydrothermal environments.

ACKNOWLEDGMENTS

We thank the captains and crews of R/V *Natsushima* and R/V *Yokosuka* as well as the operation teams of ROV *Hyper-Dolphin* and DSV *Shinkai6500* for their invaluable help in obtaining deep-sea hydrothermal vent samples. We also thank the onboard scientists, especially Shinsuke Kawagucci, Hiromi Watanabe, and Shinji Tsuchida (JAMSTEC), as well as Ko-ichi Nakamura (AIST), for their help in sample collection. We are grateful to Chong Chen and Akane Tatedou for their help in improving the manuscript.

This research was partially supported by MEXT KAKENHI (grants JP22760646 and JP26820389), TAIGA project funded by MEXT KAKENHI (grant JP20109005), and Arai Science and Technology Foundation.

This work has been performed under proposal numbers 2010B1741, 2010B1295, and 2011A1223 accepted and supported by JASRI.

FUNDING INFORMATION

This work, including the efforts of Hiroko Makita, was funded by MEXT KAKENHI (JP22760646 and JP26820389). This work, including the efforts of Ken Takai, was funded by MEXT KAKENHI (JP20109005). This work, including the efforts of Hiroko Makita, was funded by Arai Science and Technology Foundation.

REFERENCES

1. **Schwertmann U, Cornell RM.** 2000. The iron oxides in the laboratory: preparation and characterization. Wiley-VCH, New York, NY.
2. **Ehrenberg CG.** 1836. Vorläufige Mitteilungen über das wirkliche vorkommen fossiler Infusorien und ihre große Verbreitung. Poggendorff's Ann Phys Chem **38:**213–227.
3. **Winogradsky S.** 1888. Ueber Eisenbacterien. Bot Zeit **17:**262–269.
4. **Bach W, Edwards KJ.** 2003. Iron and sulfide oxidation within the basaltic ocean crust: implications for chemolithoautotrophic microbial biomass production. Geochim Cosmochim Acta **67:**3871–3887. http://dx.doi.org/10.1016/S0016-7037(03)00304-1.
5. **Bacelar-Nicolau P, Johnson DB.** 1999. Leaching of pyrite by acidophilic heterotrophic iron-oxidizing bacteria in pure and mixed cultures. Appl Environ Microbiol **65:**585–590.
6. **Rohwerder T, Gehrke T, Kinzler K, Sand W.** 2003. Bioleaching review part A: progress in bioleaching: fundamentals and mechanisms of bacterial metal sulfide oxidation. Appl Microbiol Biotechnol **63:**239–248. http://dx.doi.org/10.1007/s00253-003-1448-7.
7. **Rawlings DE, Johnson DB.** 2007. The microbiology of biomining: development and optimization of mineral-oxidizing microbial consortia. Microbiology **153:**315–324. http://dx.doi.org/10.1099/mic.0.2006/001206-0.
8. **Straub KL, Benz M, Schink B, Widdel F.** 1996. Anaerobic, nitrate-dependent microbial oxidation of ferrous iron. Appl Environ Microbiol **62:**1458–1460.
9. **Emerson D, Moyer CL.** 1997. Isolation and characterization of novel

iron-oxidizing bacteria that grow at circumneutral pH. Appl Environ Microbiol **63:**4784–4792.
10. **Baker BJ, Banfield JF.** 2003. Microbial communities in acid mine drainage. FEMS Microbiol Ecol **44:**139–152. http://dx.doi.org/10.1016/S0168-6496(03)00028-X.
11. **Edwards KJ, Bond PL, Gihring TM, Banfield JF.** 2000. An archaeal iron-oxidizing extreme acidophile important in acid mine drainage. Science **287:**1796–1799. http://dx.doi.org/10.1126/science.287.5459.1796.
12. **Edwards KJ, Rogers DR, Wirsen CO, McCollom TM.** 2003. Isolation and characterization of novel psychrophilic, neutrophilic, Fe-oxidizing, chemolithoautotrophic α- and γ-*Proteobacteria* from the deep sea. Appl Environ Microbiol **69:**2906–2913. http://dx.doi.org/10.1128/AEM.69.5.2906-2913.2003.
13. **Edwards KJ, Bach W, McCollom TM, Rogers DR.** 2004. Neutrophilic iron-oxidizing bacteria in the ocean: their habitats, diversity, and roles in mineral deposition rock alteration, and biomass production in the deep-sea. Geomicrobiol J **21:**393–404. http://dx.doi.org/10.1080/01490450490485863.
14. **Hegler F, Lösekann-Behrens T, Hanselmann K, Behrens S, Kappler A.** 2012. Influence of seasonal and geochemical changes on the geomicrobiology of an iron carbonate mineral water spring. Appl Environ Microbiol **78:**7185–7196.
15. **Klueglein N, Kappler A.** 2013. Abiotic oxidation of Fe(II) by reactive nitrogen species in cultures of the nitrate-reducing Fe(II) oxidizer *Acidovorax* sp. BoFeN1—questioning the existence of enzymatic Fe(II) oxidation. Geobiology **11:**180–190. http://dx.doi.org/10.1111/gbi.12019.
16. **Emerson D, Rentz JA, Lilburn TG, Davis RE, Aldrich H, Chan C, Moyer CL.** 2007. A novel lineage of *Proteobacteria* involved in formation of marine Fe-oxidizing microbial mat communities. PLoS One **2:**e667. http://dx.doi.org/10.1371/journal.pone.0000667.
17. **Moyer CL, Dobbs FC, Karl DM.** 1994. Estimation of diversity and community structure through restriction fragment length polymorphism distribution analysis of bacterial 16S rRNA genes from a microbial mat at an active, hydrothermal vent system, Loihi Seamount, Hawaii. Appl Environ Microbiol **60:**871–879.
18. **Moyer CL, Dobbs FC, Karl DM.** 1995. Phylogenetic diversity of the bacterial community from a microbial mat at an active, hydrothermal vent system, Loihi Seamount, Hawaii. Appl Environ Microbiol **61:**1555–1562.
19. **Davis RE, Stakes DS, Wheat CG, Moyer CL.** 2009. Bacterial variability within an iron-silica-manganese-rich hydrothermal mound located off-axis at the Cleft Segment, Juan de Fuca Ridge. Geomicrobiol J **26:**570–580. http://dx.doi.org/10.1080/01490450902889080.
20. **Davis RE, Moyer C, McAllister S, Rassa A, Tebo B.** 2010. Spatial and temporal variability of microbial communities from pre- and post-eruption microbial mats collected from Loihi Seamount, Hawaii, abstr PS.01.015. Abstr 13th Int Symp Microb Ecol, Seattle, WA, 22 to 27 August 2010.
21. **Glazer BT, Rouxel OJ.** 2009. Redox speciation and distribution within diverse iron-dominated microbial habitats at Loihi Seamount. Geomicrobiol J **26:**606–622. http://dx.doi.org/10.1080/01490450903263392.
22. **Rassa AC, McAllister SM, Safran SA, Moyer CL.** 2009. *Zeta-Proteobacteria* dominate the colonization and formation of microbial mats in low-temperature hydrothermal vents at Loihi Seamount, Hawaii. Geomicrobiol J **26:**623–638. http://dx.doi.org/10.1080/01490450903263350.
23. **Edwards KJ, Glazer BT, Rouxel OJ, Bach W, Emerson D, Davis RE, Toner BM, Chan CS, Tebo BM, Staudigel H, Moyer CL.** 2011. Ultra-diffuse hydrothermal venting supports Fe-oxidizing bacteria and massive umber deposition at 5000 m off Hawaii. ISME J **5:**1748–1758. http://dx.doi.org/10.1038/ismej.2011.48.
24. **Davis RE, Moyer CL.** 2008. Extreme spatial and temporal variability of hydrothermal microbial mat communities along the Mariana Island Arc and southern Mariana back-arc system. J Geophys Res **113:**B08S15. http://dx.doi.org/10.1029/2007JB005413.
25. **Kato S, Kobayashi C, Kakegawa T, Yamagishi A.** 2009. Microbial communities in iron-silica-rich microbial mats at deep-sea hydrothermal fields of the Southern Mariana Trough. Environ Microbiol **11:**2094–2111. http://dx.doi.org/10.1111/j.1462-2920.2009.01930.x.
26. **Kato S, Yanagawa K, Sunamura M, Takano Y, Ishibashi J, Kakegawa T, Utsumi M, Yamanaka T, Toki T, Noguchi T, Kobayashi K, Moroi A, Kimura H, Kawarabayasi Y, Marumo K, Urabe T, Yamagishi A.** 2009. Abundance of *Zetaproteobacteria* within crustal fluids in back-arc hydrothermal fields of the Southern Mariana Trough. Environ Microbiol **11:**3210–3222. http://dx.doi.org/10.1111/j.1462-2920.2009.02031.x.
27. **Staudigel H, Hart SR, Pile A, Bailey BE, Baker ET, Brooke S, Connelly DP, Haucke L, German CR, Hudson I, Jones D, Koppers AA, Konter J, Lee R, Pietsch TW, Tebo BM, Templeton AS, Zierenberg R, Young CM.** 2006. Vailulu'u Seamount, Samoa: life and death on an active submarine volcano. Proc Natl Acad Sci U S A **103:**6448–6453. http://dx.doi.org/10.1073/pnas.0600830103.
28. **Sudek LA, Templeton AS, Tebo BM, Staudigel H.** 2009. Microbial ecology of Fe (hydr)oxide mats and basaltic rock from Vailulu'u Seamount, American Samoa. Geomicrobiol J **26:**581–596. http://dx.doi.org/10.1080/01490450903263400.
29. **Hodges TW, Olson JB.** 2009. Molecular comparison of bacterial communities within iron-containing flocculent mats associated with submarine volcanoes along the Kermadec Arc. Appl Environ Microbiol **75:**1650–1657. http://dx.doi.org/10.1128/AEM.01835-08.
30. **Forget NL, Murdock SA, Juniper SK.** 2010. Bacterial diversity in Fe-rich hydrothermal sediments at two South Tonga Arc submarine volcanoes. Geobiology **8:**417–432. http://dx.doi.org/10.1111/j.1472-4669.2010.00247.x.
31. **Alt JC.** 1988. Hydrothermal oxide and nontronite deposits on seamounts in the eastern Pacific. Mar Geol **81:**227–239. http://dx.doi.org/10.1016/0025-3227(88)90029-1.
32. **Bogdanov YA, Lisitzin AP, Binns RA, Gorshkov AI, Gurvich EG, Dritz VA, Dubinina GA, Bogdanova OY, Sivkov AV, Kuptsov VM.** 1997. Low-temperature hydrothermal deposits of Franklin Seamount, Woodlark Basin, Papua New Guinea. Mar Geol **142:**99–117. http://dx.doi.org/10.1016/S0025-3227(97)00043-1.
33. **Juniper SK, Fouquet Y.** 1988. Filamentous iron-silica deposits from modern and ancient hydrothermal sites. Can Mineral **26:**859–869.
34. **Kennedy CB, Scott SD, Ferris FG.** 2003. Ultrastructure and potential sub-seafloor evidence of bacteriogenic iron oxides from Axial Volcano, Juan de Fuca Ridge, north-east Pacific Ocean. FEMS Microbiol Ecol **43:**247–254. http://dx.doi.org/10.1111/j.1574-6941.2003.tb01064.x.
35. **Kennedy CB, Martinez RE, Scott SD, Ferris FG.** 2003. Surface chemistry and reactivity of bacteriogenic iron oxides from Axial Volcano, Juan de Fuca Ridge, north-east Pacific Ocean. Geobiology **1:**59–69. http://dx.doi.org/10.1046/j.1472-4669.2003.00001.x.
36. **Kennedy CB, Scott SD, Ferris FG.** 2003. Characterization of bacteriogenic iron oxide deposits from Axial Volcano, Juan de Fuca Ridge, North-east Pacific Ocean. Geomicrobiol J **20:**199–214. http://dx.doi.org/10.1080/01490450303873.
37. **McBeth JM, Little BJ, Ray RI, Farrar KM, Emerson D.** 2011. Neutrophilic iron-oxidizing "*Zetaproteobacteria*" and mild steel corrosion in nearshore marine environments. Appl Environ Microbiol **77:**1405–1412. http://dx.doi.org/10.1128/AEM.02095-10.
38. **Emerson D, Moyer CL.** 2002. Neutrophilic Fe-oxidizing bacteria are abundant at the Loihi Seamount hydrothermal vents and play a major role in Fe oxide deposition. Appl Environ Microbiol **68:**3085–3093. http://dx.doi.org/10.1128/AEM.68.6.3085-3093.2002.
39. **Chan CS, Fakra SC, Emerson D, Fleming EJ, Edwards KJ.** 2011. Lithotrophic iron-oxidizing bacteria produce organic stalks to control mineral growth: implications for biosignature formation. ISME J **5:**717–727. http://dx.doi.org/10.1038/ismej.2010.173.
40. **Pringsheim EG.** 1949. Iron bacteria. Biol Rev Camb Philos Soc **24:**200–245. http://dx.doi.org/10.1111/j.1469-185X.1949.tb00575.x.
41. **Kucera S, Wolfe RS.** 1957. A selective enrichment method for *Gallionella ferruginea*. J Bacteriol **74:**344–349.
42. **Ghiorse WC.** 1984. Biology of iron- and manganese-depositing bacteria. Annu Rev Microbiol **38:**515–550. http://dx.doi.org/10.1146/annurev.mi.38.100184.002503.
43. **Hallbeck L, Pedersen K.** 1990. Culture parameters regulating stalk formation and growth rate of *Gallionella ferruginea*. J Gen Microbiol **136:**1675–1680. http://dx.doi.org/10.1099/00221287-136-9-1675.
44. **Hallbeck L, Pedersen K.** 1991. Autotrophic and mixotrophic growth of *Gallionella ferruginea*. J Gen Microbiol **137:**2657–2661. http://dx.doi.org/10.1099/00221287-137-11-2657.
45. **Hallbeck L, Ståhl F, Pederson K.** 1993. Phylogeny and phenotypic characterization of the stalk-forming and iron-oxidizing bacterium *Gallionella ferruginea*. J Gen Microbiol **139:**1531–1535.
46. **Hallberg R, Ferris FG.** 2004. Biomineralization by *Gallionella*. Geomicrobiol J **21:**325–330. http://dx.doi.org/10.1080/01490450490454001.
47. **Hanert HH.** 2006. The genus *Gallionella*, p 990–995. *In* Dworkin M,

Falkow S, Rosenberg E, Schleifer KH, Stackebrandt E (ed), The prokaryotes, vol 7. Springer, New York, NY.
48. **halbach M, Koschinsky A, Halbach P.** 2001. Report of the discovery of *Gallionella ferruginea* from an active hydrothermal field in the deep sea. InterRidge News **10:**18–20.
49. **Singer E, Emerson D, Webb EA, Barco RA, Kuenen JG, Nelson WC, Chan CS, Comolli LR, Ferriera S, Johnson J, Heidelberg JF, Edwards KJ.** 2011. *Mariprofundus ferrooxydans* PV-1 the first genome of a marine Fe(II) oxidizing zetaproteobacterium. PLoS One **6:**e25386. http://dx.doi.org/10.1371/journal.pone.0025386.
50. **McAllister SM, Davis RE, McBeth JM, Tebo BM, Emerson D, Moyer CL.** 2011. Biodiversity and emerging biogeography of the neutrophilic iron-oxidizing *Zetaproteobacteria*. Appl Environ Microbiol **77:**5445–5457. http://dx.doi.org/10.1128/AEM.00533-11.
51. **Emerson D, Moyer CL.** 2010. Microbiology of seamounts: common patterns observed in community structure. Oceanography **23:**148–163. http://dx.doi.org/10.5670/oceanog.2010.67.
52. **Nakamura K, Toki T, Mochizuki N, Asada M, Ishibashi J, Nogi Y, Yoshikawa S, Miyazaki J, Okino K.** 2013. Discovery of a new hydrothermal vent based on an underwater, high-resolution geophysical survey. Deep-Sea Res Part I Oceanogr Res Pap **74:**1–10. http://dx.doi.org/10.1016/j.dsr.2012.12.003.
53. **Yamanaka T, Nagashio H, Nishio R, Kondo K, Noguchi T, Okamura K, Nunoura T, Makita H, Nakamura K, Watanabe H, Inoue K, Toki T, Iguchi K, Tsunogai U, Nakada R, Ohshima S, Toyoda S, Kawai J, Yoshida N, Ijira A, Sunamura M.** 2015. Tarama Knoll: geochemical and biological profiles of hydrothermal activity, p 497–504. *In* Ishibashi J, Okino K, Sunamura M (ed), Subseafloor biosphere linked to hydrothermal systems: TAIGA concept. Springer Japan, Tokyo, Japan.
54. **Masuda H, Fryer P, Ishibashi J, Toki T, Shitashima K, Kimura H, Suzuki R, Sato S, Takemoto K, Kato S, Kobayashi C, Kuno M, Noguchi T, Aoki M.** 2005. YK05-09 Leg2: *Shinkai6500*/*Yokosuka* cruise report. Japan Agency for Marine-Earth Science and Technology, Yokosuka Kanagawa Prefecture, Japan. http://www.godac.jamstec.go.jp/catalog/data/doc_catalog/media/YK05-09_leg2_all.pdf.
55. **Saegusa S, Tsunogai U, Nakagawa F, Kaneko S.** 2006. Development of a multibottle gas-tight fluid sampler WHATS II for Japanese submersibles/ROVs. Geofluids **6:**234–240. http://dx.doi.org/10.1111/j.1468-8123.2006.00143.x.
56. **Trüper HG, Schlegel HG.** 1964. Sulfur metabolism in *Thiorhodaceae* I. Quantitative measurements on growing cells of *Chromatium okenii*. Antonie Van Leeuwenhoek **30:**225–238.
57. **Crosby NT.** 1968. Determination of ammonia by the Nessler method in waters containing hydrazine. Analyst **93:**406–408.
58. **Harvey AE, Smart JA, Amis ES.** 1955. Simultaneous spectrophotometric determination of iron(II) and total iron with 1,10-phenanthroline. Anal Chem **27:**26–29. http://dx.doi.org/10.1021/ac60097a009.
59. **Kikuchi S, Makita H, Takai K, Yamaguchi N, Takahashi Y.** 2014. Characterization of biogenic iron oxides collected by the newly designed liquid culture method using diffusion chambers. Geobiology **12:**133–145. http://dx.doi.org/10.1111/gbi.12073.
60. **Lunau M, Lemke A, Walther K, Martens-Habbena W, Simon M.** 2005. An improved method for counting bacteria from sediments and turbid environments by epifluorescence microscopy. Environ Microbiol **7:**961–968. http://dx.doi.org/10.1111/j.1462-2920.2005.00767.x.
61. **Porter KG, Feig YS.** 1980. The use of DAPI for identifying and counting microflora. Limnol Oceanogr **25:**943–948. http://dx.doi.org/10.4319/lo.1980.25.5.0943.
62. **Lane DJ.** 1991. 16S/23S rRNA sequencing, p 115–175. *In* Stackebrandt E, Goodfellow M (ed), Nucleic acid techniques in bacterial systematics. John Wiley & Sons, Chichester, United Kingdom.
63. **Altschul SF, Madden TL, Schaffer AA, Zhang J, Zhang Z, Miller W, Lipman DJ.** 1997. Gapped BLAST and PSI-BLAST: a new generation of protein database search programs. Nucleic Acids Res **25:**3389–3402. http://dx.doi.org/10.1093/nar/25.17.3389.
64. **Cole JR, Wang Q, Cardenas E, Fish J, Chai B, Farris RJ, Kulam-Syed-Mohideen AS, McGarrell DM, Marsh T, Garrity GM, Tiedje JM.** 2009. The Ribosomal Database Project: improved alignments and new tools for rRNA analysis. Nucleic Acids Res **37:**141–145. http://dx.doi.org/10.1093/nar/gkn879.
65. **Cole JR, Chai B, Farris RJ, Wang Q, Kulam SA, McGarrell DM, Garrity GM, Tiedje JM.** 2005. The Ribosomal Database Project (RDP-II): sequences and tools for high-throughput rRNA analysis. Nucleic Acids Res **33:**D294–D296. http://dx.doi.org/10.1093/nar/gki038.
66. **Ludwig W, Strunk O, Westram R, Richter L, Meier H, Yadhukumar Buchner A, Lai T, Steppi S, Jobb G, Forster W, Brettske I, Gerber S, Ginhart AW, Gross O, Grumann S, Hermann S, Jost R, Konig A, Liss T, Lussmann R, May M, Nonhoff B, Reichel B, Strehlow R, Stamatakis A, Stuckmann N, Vilbig A, Lenke M, Ludwig T, Bode A, Schleifer KH.** 2004. ARB: a software environment for sequence data. Nucleic Acids Res **32:**1363–1371. http://dx.doi.org/10.1093/nar/gkh293.
67. **Tamura K, Peterson D, Peterson N, Stecher G, Nei M, Kumar S.** 2011. MEGA5: molecular evolutionary genetics analysis using maximum likelihood, evolutionary distance, and maximum parsimony methods. Mol Biol Evol **28:**2731–2739. http://dx.doi.org/10.1093/molbev/msr121.
68. **Saitou N, Nei M.** 1987. The neighbor-joining method: a new method for reconstructing phylogenetic trees. Mol Biol Evol **4:**406–425.
69. **Felsenstein J.** 1981. Evolutionary trees from DNA sequences: a maximum likelihood approach. J Mol Evol **17:**368–376.
70. **Altschul SF, Gish W, Miller W, Meyers EW, Lipman DJ.** 1990. Basic local alignment search tool. J Mol Biol **215:**403–410. http://dx.doi.org/10.1016/S0022-2836(05)80360-2.
71. **Takai K, Horikoshi K.** 2000. Rapid detection and quantification of members of the archaeal community by quantitative PCR using fluorogenic probes. Appl Environ Microbiol **66:**5066–5072. http://dx.doi.org/10.1128/AEM.66.11.5066-5072.2000.
72. **Lupton J, Butterfield D, Lilley M, Evans L, Nakamura K, Chadwick W, Jr, Resing J, Embley R, Olson E, Proskurowski G, Baker E, de Ronde C, Roe K, Greene R, Lebon G, Young C.** 2006. Submarine venting of liquid carbon dioxide on a Mariana Arc volcano. Geochem Geophys Geosyst **7:**Q0800. http://dx.doi.org/101029/2005GC001152.
73. **Embley RW, Baker ET, Butterfield DA, Chadwick WW, Jr, Lupton JE, Resing JA, De Ronde CEJ, Nakamura K, Tunnicliffe V, Dower J, Merle SG.** 2007. Exploring the submarine ring of fire Mariana Arc–Western Pacific. Oceanography **20:**68–79. http://dx.doi.org/10.5670/oceanog.2007.07.
74. **Nakamura K, Inagaki F, Embley RW, Tsuchida S, Lilley MD, Lupton JE, Roe K, Gena K, Nakagawa S, Lipp J, Yamaguchi H, Dower JF.** 2006. Blue Earth 2006, abstract S25. https://www.jamstec.go.jp/maritec/j/blueearth/2006/yokou/S25.pdf.
75. **Wheat CG, Fryer P, Hulme S, Becker N, Curtis A, Moyer C.** 2003. Hydrothermal venting in the southern most portion of the Mariana back-arc spreading center at 12.57 degrees N, abstr T32A-0920. Am Geophys Union Fall Meet, San Francisco, CA, 8 to 12 December 2003.
76. **Ishibashi J, Yamanaka T, Kimura H, Hirota A, Toki T, Tsunogai U, Gamo T, Utsumi M, Roe K, Miyabe S, Okamura K.** 2004. Geochemistry of hydrothermal fluids in south Mariana backarc spreading center, abstr V44A-05. Am Geophys Union Fall Meet, San Francisco, CA, 13 to 17 December 2004.
77. **Baker ET, Massoth GJ, Nakamura K, Embley RW, De Ronde CEJ, Arculus RJ.** 2005. Hydrothermal activity on near-arc sections of back-arc ridges: results from the Mariana Trough and Lau Basin. Geochem Geophys Geosyst **6:**Q09001. http://dx.doi.org/10.1029/2005GC000948.
78. **Matsuno T, Kimura M, Seama N.** 2015. Electrical resistivity structure of the Snail hydrothermal site at the Southern Mariana Trough spreading center, p 241–251. *In* Ishibashi J, Okino K, Sunamura S (ed), Subseafloor biosphere linked to global hydrothermal systems: TAIGA concept. Springer Japan, Tokyo, Japan.
79. **Seama N, Okino K.** 2015. Asymmetric seafloor spreading of the Southern Mariana Trough back-arc basin, p 53–260. *In* Ishibashi J, Okino K, Sunamura S (ed), Subseafloor biosphere linked to global hydrothermal systems: TAIGA concept. Springer Japan, Tokyo, Japan.
80. **Seama N, Sato H, Nogi Y, Okino K.** 2015. The mantle dynamics, the crustal formation, and the hydrothermal activity of the Southern Mariana Trough back-arc basin, p 215–227. *In* Ishibashi J, Okino K, Sunamura S (ed), Subseafloor biosphere linked to global hydrothermal systems: TAIGA concept. Springer Japan, Tokyo, Japan.
81. **Kikuchi S, Makita H, Mitsunobu S, Terada Y, Yamaguchi N, Takai K, Takahashi Y.** 2011. Application of synchrotron based μ-XRF-XAFS to the speciation of Fe on single stalk in bacteriogenic iron oxides (BIOS). Chem Lett **40:**680–681. http://dx.doi.org/10.1246/cl.2011.680.
82. **Suzuki T, Hashimoto H, Matsumoto N, Furutani M, Kunoh H, Takada H.** 2011. Nanometer-scale visualization and structural analysis of the inorganic/organic hybrid structure of *Gallionella ferruginea* twisted stalks.

Appl Environ Microbiol **77:**2877–2881. http://dx.doi.org/10.1128/AEM.02867-10.

83. **Suzuki T, Hashimoto H, Itadani A, Matsumoto N, Kunoh H, Takada J.** 2012. Silicon and phosphorus linkage with iron via oxygen in the amorphous matrix of *Gallionella ferruginea* stalks. Appl Environ Microbiol **78:**236–241. http://dx.doi.org/10.1128/AEM.05913-11.
84. **Manceau A, Drits VA.** 1993. Local structure of ferrihydrite and feroxyhite by EXAFS spectroscopy. Clay Miner **28:**165–184. http://dx.doi.org/10.1180/claymin.1993.028.2.01.
85. **Mitsunobu S, Shiraishi F, Makita H, Orchtt B, Kikuchi S, Jorgensen B, Takahashi Y.** 2012. Bacteriogenic Fe(III) (oxyhydr)oxides characterized by synchrotron microprobe coupled with spatially resolved phylogenetic analysis. Environ Sci Technol **46:**3304–3311. http://dx.doi.org/10.1021/es203860m.
86. **Toner MB, Santelli CM, Marcus MA, Wirth R, Chan CS, McCollom T, Bach W, Edwards KJ.** 2009. Biogenic iron oxyhydroxide formation at mid-ocean ridge hydrothermal vents: Juan de Fuca Ridge. Geochim Cosmochim Acta **73:**388–403. http://dx.doi.org/10.1016/j.gca.2008.09.035.
87. **Fuchida S, Mizuno Y, Masuda H, Toki T, Makita H.** 2014. Concentrations and distributions of amino acids in black and white smoker fluids at temperatures over 200°C. Org Geochem **66:**98–106. http://dx.doi.org/10.1016/j.orggeochem.2013.11.008.
88. **Noguchi T, Fukuba T, Okamura K, Ijiri A, Yanagawa K, Ishitani Y, Fujii T, Sunamura M.** 2015. Distribution and biogeochemical properties of hydrothermal plumes in the Rodriguez Triple Junction, p 195–204. *In* Ishibashi J, Okino K, Sunamura S (ed), Subseafloor biosphere linked to global hydrothermal systems: TAIGA concept. Springer Japan, Tokyo, Japan.
89. **Könneke M, Bernhard AE, de la Torre JR, Walker CB, Waterbury JB, Stahl DA.** 2005. Isolation of an autotrophic ammonia-oxidizing marine archaeon. Nature **437:**543–546. http://dx.doi.org/10.1038/nature03911.
90. **Heck KL, Jr, Van Belle G, Simberloff D.** 1975. Explicit calculation of the rarefaction diversity measurement and the determination of sufficient sample size. Ecology **56:**1459–1461. http://dx.doi.org/10.2307/1934716.
91. **Schloss PD, Handelsman J.** 2005. Introducing DOTUR, a computer program for defining operational taxonomic units and estimating species richness. Appl Environ Microbiol **71:**1501–1506. http://dx.doi.org/10.1128/AEM.71.3.1501-1506.2005.
92. **Hirayama H, Suzuki Y, Abe M, Miyazaki M, Makita H, Inagaki F, Uematsu K, Takai K.** 2011. *Methylothermus subterraneus* sp. nov., a moderately thermophilic methanotroph isolated from a terrestrial subsurface hot aquifer. Int J Syst Evol Microbiol **61:**2646–2653. http://dx.doi.org/10.1099/ijs.0.028092-0.
93. **Emerson D, Ghiorse WC.** 1993. Ultrastructure and chemical composition of the sheath of *Leptothrix discophora* SP-6. J Bacteriol **175:**7808–7818.
94. **Wu W, Swanner ED, Hao L, Zeitvogel F, Obst M, Pan Y, Kappler A.** 2014. Characterization of the physiology and cell-mineral interactions of the marine anoxygenic phototrophic Fe(II) oxidizer *Rhodovulum iodosum*—implications for Precambrian Fe(II) oxidation. FEMS Microbiol Ecol **88:**503–515. http://dx.doi.org/10.1111/1574-6941.12315.
95. **Toner MB, Berquo T, Michel FM, Sorensen JV, Templeton AS, Edwards KJ.** 2012. Mineralogy of iron microbial mats from Loihi Seamount. Front Microbiol **3:**118. http://dx.doi.org/10.3389/fmicb.2012.00118.
96. **García-Ruiz JM, Hyde ST, Carnerup AM, Christy AG, Van Kranendonk MJ, Welham NJ.** 2003. Self-assembled silica-carbonate structures and detection of ancient microfossils. Science **302:**1194–1197. http://dx.doi.org/10.1126/science.1090163.
97. **García-Ruiz JM, Melero-García E, Hyde ST.** 2009. Morphogenesis of self-assembled nanocrystalline materials of barium carbonate and silica. Science **323:**362–365. http://dx.doi.org/10.1126/science.1165349.
98. **Urabe T, Ishibashi J, Sunamura M, Okino K, Takai K, Suzuki K.** 2015. Introduction of TAIGA concept, p 1–3. *In* Ishibashi J, Okino K, Sunamura S (ed), Subseafloor biosphere linked to global hydrothermal systems: TAIGA concept. Springer Japan, Tokyo, Japan.
99. **Picard A, Kappler A, Schmid G, Quaroni L, Obst M.** 2015. Experimental diagenesis of organo-mineral structures formed by microaerophilic Fe(II)-oxidizing bacteria. Nat Commun **6:**6277. http://dx.doi.org/10.1038/ncomms7277.